Numerical modeling of the machining behavior of natural fiber composites

1. **Faissal Chegdani** *

   - Arts et Metiers Institute of Technology, MSMP, HESAM Université, F-51006, Châlons-en-Champagne, France.

   Email: faissal.chegdani@ensam.eu

2. **Mohamed El Mansori**

   - Arts et Metiers Institute of Technology, MSMP, HESAM Université, F-51006, Châlons-en-Champagne, France
   - Texas A&M Engineering Experiment Station, Institute for Manufacturing Systems, College Station, TX 77843, USA

   Email: mohamed.elmansori@ensam.eu

ABSTRACT: (50-100 words)

This chapter presents a 2D micromechanical model developed to predict the machining behavior of natural fiber composites using the finite element (EF) method. Natural fibers are modeled using an elasto-plastic behavior and a ductile criterion for failure. The FE model has been performed for the orthogonal cutting of flax fiber reinforced polymer composites. Results shows a good predictiveness of the qualitative cutting behavior of flax fibers. However, correlation issues were noticed on the predictiveness of thrust forces. The FE has been then improved through a tribological approach based on the local micro-friction between the cutting toot and each composite component.

KEYWORDS: (10-15 keywords)

Natural fiber composites; Machining; Finite element modeling; Cohesive zone modeling; Ductile damage criterion; Cutting speed; Fiber orientation; Micro-friction; Cutting force; Thrust force.

* Corresponding author

1. Introduction

Machining of natural fiber composites (NFC) starts arousing the interest of many researchers due to the increase in the use of NFC materials in different industrial applications (Lotfi et al., 2019; Nassar et al., 2017; Rajmohan et al., 2019; Roy Choudhury et al., 2018; Vinayagamoorthy and Rajmohan, 2018). The machinability of NFC has shown different technical issues related to the well-known complex multiscale cellulosic structure of natural fibers (Baley, 2002). Indeed, the machining behavior of NFC is highly sensitive to the small variation of material and process parameters (Chegdani et al., 2018a, 2016; F. Chegdani et al., 2015; Faissal Chegdani et al., 2015; Chegdani and El Mansori, 2018; Chegdani and Mansori, 2018). Moreover, a new multiscale approach has been developed to perform the machinability qualification of NFC materials. This approach postulates that the machining investigation of NFC requires the selection of the pertinent analysis scale that corresponds to the size of the natural fibrous reinforcement structure (Chegdani and El Mansori, 2019).

Despite the effectiveness of the new machinability qualification approach for NFC, its application presents some issues related to the high variability of natural fibers in terms of shape and diameter (Hossain et al., 2013). Therefore, the new multiscale approach should be adapted and re-applied to each fibers harvest because, depending on the environmental conditions of growth, the fibrous structure size could vary significantly which is time and cost consuming for the experimental machinability qualification.

The use of the numerical technologies could be an efficient way to resolve these issues. Indeed, developing a numerical model for machining of NFC could reduce considerably the time and the cost of the machinability analysis during the experimental validation of new NFC products. For this aim, this chapter proposes a 2D micromechanical finite element model to simulate the orthogonal cutting behavior of NFC at the pertinent scale of natural fibers.

Finite element (FE) method has previously been applied to model the machining behavior of synthetic fiber composites at microscale (Dandekar and Shin, 2012, 2008; Gao et al., 2016; Rao et al., 2007; Venu Gopala Rao et al., 2007). All the FE models are developed for synthetic fiber reinforced thermoset composites because of their heavy use in structural industrial applications. Synthetic fibers have been modeled with an elastic behavior and brittle failure based on the maximum failure stress criterion. Polymer matrices have been modeled with an elasto-plastic behavior and a ductile damage. Interfaces have been usually modeled with the cohesive zone model (CZM) while some researchers consider the interfaces as solid continuum elements (Gao et al., 2016).

For NFC materials, natural fibers cannot be modeled using the maximum failure stress criterion at microscale. This is because natural fibers have a cellulosic structure that induces a visco-elasto-plastic behavior with both tensile tests (Charlet et al., 2007; Placet et al., 2014) and nanoindentation experiments (Chegdani et al., 2018b, 2017; Keryvin et al., 2015). Also, the well-known Jonson-cook model for ductile materials (Johnson and Cook, 1985) cannot be applied to natural fibers because it assumes an isotropic hardening of the considered material ("Abaqus Analysis User's Manual," 2011), while natural fibers show an anisotropic behavior (Baley, 2002).

In this chapter, the FE machining model will be developed for natural fibers reinforced thermoplastic composites that are the most used in the industry to insure the recyclability of these eco-friendly materials.

2. Finite element modeling strategy

2.1. Finite element model setup

Figure 1 shows the geometrical setup of the FE model carried out using ABAQUS/Explicit software (version 6.11-2) ("Abaqus Analysis User's Manual," 2011). The microscopic-based model consists of a bundle of four elementary flax fibers embedded in the polymer matrix. The interfaces between flax fibers and the matrix are modeled with cohesive elements that have a thickness of 1 μm. Each elementary fiber has a diameter of 15 μm. The cutting tool is considered as an analytical rigid body where the movement is controlled by a reference point. Flax fibers are oriented with an angle "θ" from the cutting direction. A plane stress analysis, which is more suitable for FEM cutting of composites (Lasri et al., 2009), is considered in this numerical investigation. Both flax fibers and PP matrix are meshed with 4-node bilinear plane stress quadrilateral elements (CPS4R) and 2 μm of mesh size. Cohesive interfaces are meshed with a 4-node two-dimensional cohesive element (COH2D4) and 1 μm of mesh size. As for synthetic fiber composites, the thermal effect is not considered in this micromechanical study because the heat generation in orthogonal cutting requires a large cutting length (Nayak et al., 2004; Santiuste et al., 2010). The cutting length in the current model does not exceed 200 μm.

Two NFC materials are considered in this chapter to model the machining behavior:

- Unidirectional flax fiber reinforced polypropylene composite (Flax/PP);
- Unidirectional flax fiber reinforced polylactic-acid composite (Flax/PLA).

Next section will describe the modeling laws used for each composite component.

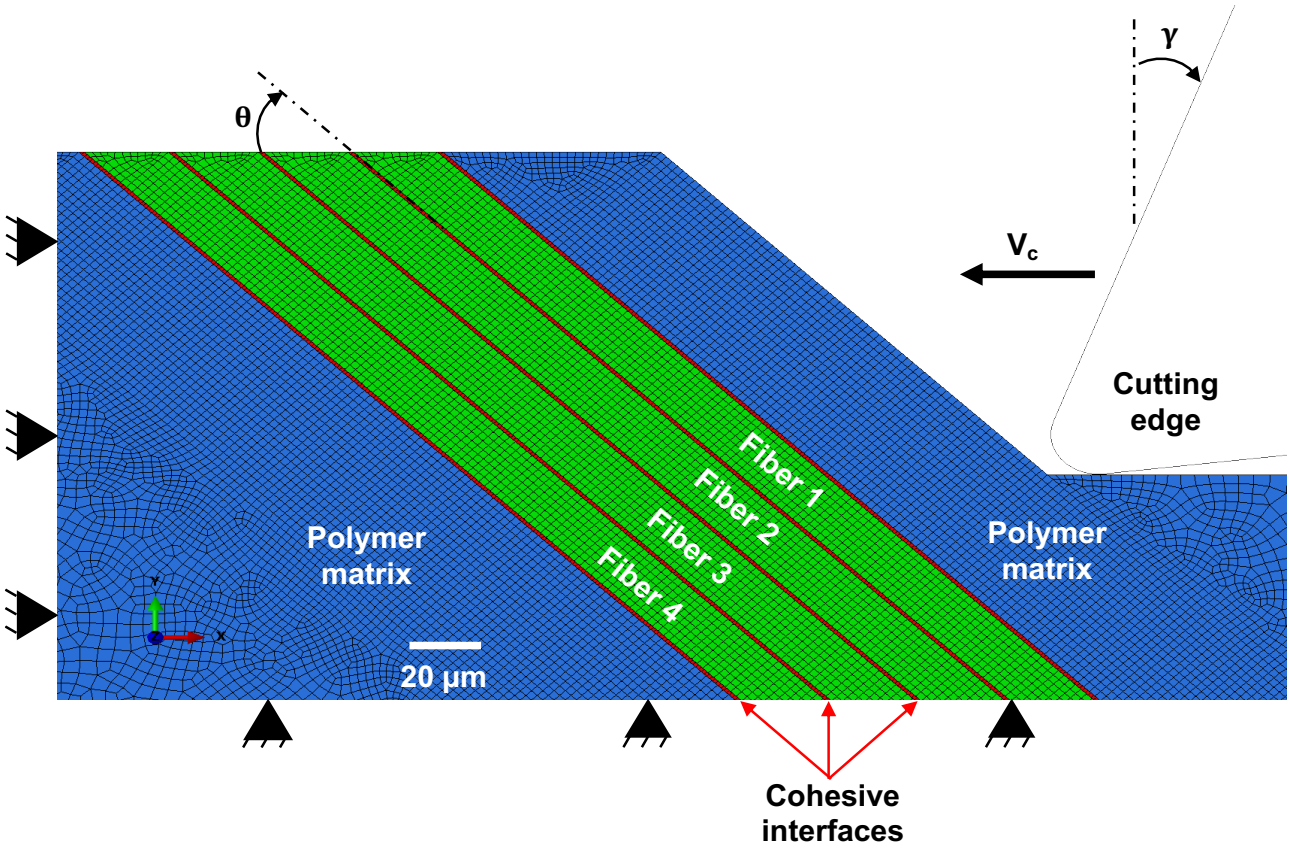

Figure 1 : Geometrical setup of the micromechanical EF model for machining NFC

2.2. Finite element modeling of natural fibers

Unlike synthetic fibers such glass and carbon, natural fibers exhibit an anisotropic behavior due to their cellulosic structure as shown in Figure 2(a) where natural fibers are structured as a stacking of cell walls and each cell wall is itself a composite material of cellulose microfibrils embedded in natural amorphous polymers of hemicellulose, pectin, and lignin (Baley, 2002; Charlet et al., 2007). The major cell wall that controls the fiber behavior is “S2” because of its predominant volume. In the cell wall S2, the cellulose microfibrils are oriented with a small angle called the microfibrillar angle (MFA) (Baley, 2002).

This cellulosic structure of natural fibers induces an orthotropic behavior and the mechanical behavior of the elementary flax fiber depends on the cellulose microfibrils orientation toward the fiber axis. Indeed, tensile tests on elementary flax fibers show a non-linearity in the

stress/strain curve as shown in Figure 2(b) and three specific behaviors are discriminated in the curve as follows (Baley, 2002; Charlet et al., 2007):

- First linear elastic behavior that corresponds to first mechanical response of the initial cellulose microfibrils structure;
- Non-linear plastic behavior that corresponds to rearrangement of cellulose microfibrils by the tensile motion to be as parallel as possible to the fiber axis;
- Second linear elastic behavior that corresponds to the second mechanical response of the cellulose microfibrils structure after rearrangement.

The alignment of cellulose microfibrils induces rearrangements in the core of the surrounding amorphous polymers and, therefore, the cellulosic reorganization implies an elasto-visco-plastic deformation (Charlet et al., 2007). Consequently, natural fibers cannot be modeled as synthetic fibers (glass and carbon) using an elastic behavior. In the case of flax fibers, a plastic behavior should be considered before fiber failure for the FE model.

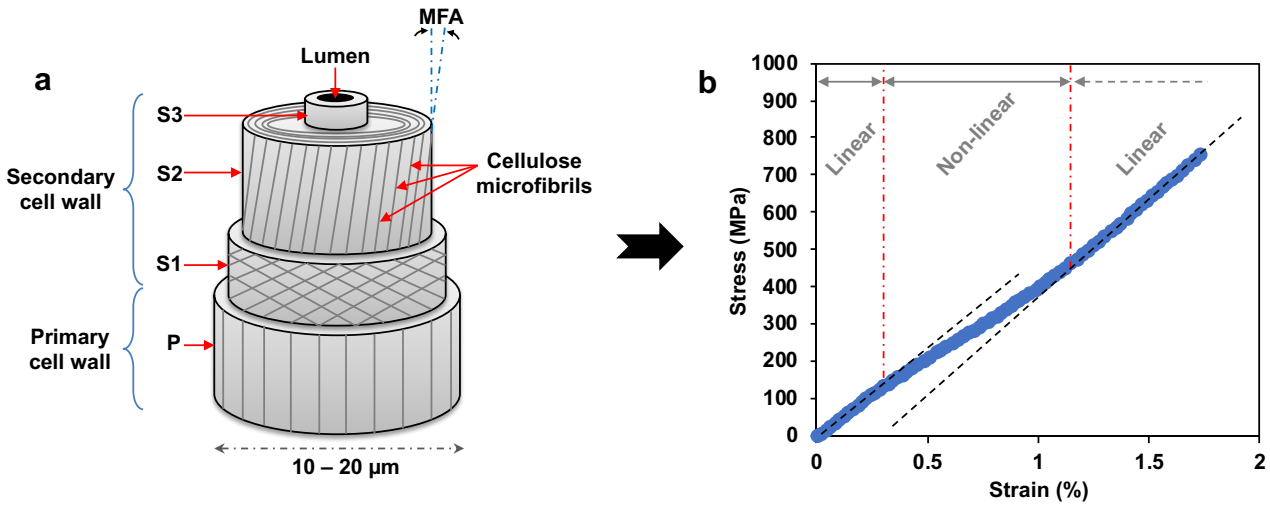

Figure 2: (a) Schematic illustration of the cellulosic structure of an elementary flax fiber. (b) Typical stress/strain curve of elementary flax fiber (adapted from (Shah et al., 2012))

Natural fibers show a high variability of their mechanical properties for the same reasons shape a diameter variability discussed in Section 1. For flax fibers, the literature gives a tensile modulus from 27 GPa to 103 GPa, a tensile strength from 343 MPa to 2000 MPa, and an elongation from 1.2 % to 3.3 % (Dittenber and GangaRao, 2012). Flax fiber shear strength

has been found between 10 MPa and 50 MPa (Panamoottil et al., 2017). Therefore, the considered mechanical parameters should be chosen to be as closer as possible to those of flax fibers used in the experimental validation of the model. Table 1 summarizes the considered mechanical parameters for flax fibers.

The longitudinal plastic behavior of flax fibers is implemented using 30 points on the yield stress versus plastic strain curve from Figure 2(b) with a maximum yield stress of 750 MPa. To model the anisotropic plasticity-based failure for flax fibers, the Hill's potential function is used (Cardoso and Adetoro, 2017). Hill's potential function is a simple extension of the Mises function, which can be expressed in terms of rectangular Cartesian stress components (σ_{ij}) as following ("Abaqus Analysis User's Manual," 2011; Panamoottil et al., 2017):

$$f(\sigma) = \sqrt{F(\sigma_{22} - \sigma_{33})^2 + G(\sigma_{33} - \sigma_{11})^2 + H(\sigma_{11} - \sigma_{22})^2 + 2L\sigma_{23}^2 + 2M\sigma_{31}^2 + 2N\sigma_{12}^2} \quad (1)$$

Where *F, G, H, L, M* and *N* are constants defined as following:

$$F = \frac{(\sigma^0)^2}{2}\left(\frac{1}{\bar{\sigma}_{22}^2} + \frac{1}{\bar{\sigma}_{33}^2} + \frac{1}{\bar{\sigma}_{11}^2}\right) = \frac{1}{2}\left(\frac{1}{R_{22}^2} + \frac{1}{R_{33}^2} + \frac{1}{R_{11}^2}\right) \quad (2)$$

$$G = \frac{(\sigma^0)^2}{2}\left(\frac{1}{\bar{\sigma}_{33}^2} + \frac{1}{\bar{\sigma}_{11}^2} - \frac{1}{\bar{\sigma}_{22}^2}\right) = \frac{1}{2}\left(\frac{1}{R_{33}^2} + \frac{1}{R_{11}^2} - \frac{1}{R_{22}^2}\right) \quad (3)$$

$$H = \frac{(\sigma^0)^2}{2}\left(\frac{1}{\bar{\sigma}_{11}^2} + \frac{1}{\bar{\sigma}_{22}^2} - \frac{1}{\bar{\sigma}_{33}^2}\right) = \frac{1}{2}\left(\frac{1}{R_{11}^2} + \frac{1}{R_{22}^2} - \frac{1}{R_{33}^2}\right) \quad (4)$$

$$L = \frac{3}{2}\left(\frac{\tau^0}{\bar{\sigma}_{23}}\right)^2 = \frac{3}{2R_{23}^2} \quad (5)$$

$$M = \frac{3}{2}\left(\frac{\tau^0}{\bar{\sigma}_{13}}\right)^2 = \frac{3}{2R_{13}^2} \quad (6)$$

$$N = \frac{3}{2}\left(\frac{\tau^0}{\bar{\sigma}_{12}}\right)^2 = \frac{3}{2R_{12}^2} \quad (7)$$

where each $\bar{\sigma}_{ij}$ is the measured yield stress value when σ_{ij} is applied as the only nonzero stress component, $\tau^0 = \frac{\sigma_0}{\sqrt{3}}$ where σ_0 is the reference yield stress which is set to be equal to

σ_{11}in this case; R_{ij} are anisotropic yield stress ratios that are needed to implement the Hill's potential function in the FE model ("Abaqus Analysis User's Manual," 2011) and are defined as follows where the considered strength values are provided in Table 1:

$$R_{11} = \frac{\bar{\sigma}_{11}}{\sigma^0} \tag{8}$$

$$R_{22} = \frac{\bar{\sigma}_{22}}{\sigma^0} \tag{9}$$

$$R_{33} = \frac{\bar{\sigma}_{33}}{\sigma^0} \tag{10}$$

$$R_{12} = \frac{\bar{\sigma}_{12}}{\tau^0} \tag{11}$$

$$R_{13} = \frac{\bar{\sigma}_{13}}{\tau^0} \tag{12}$$

$$R_{23} = \frac{\bar{\sigma}_{23}}{\tau^0} \tag{13}$$

A ductile criterion (Hooputra et al., 2004) is considered to model the failure of flax fibers. The ductile criterion is based on a fracture diagram which gives the equivalent plastic strain at fracture as a function of the stress state. The model assumes that the equivalent plastic strain at the onset of damage is a function of stress triaxiality and strain rate. The criterion for damage initiation is met when the following condition is satisfied (Hooputra et al., 2004):

$$\int_0^{\varepsilon_{eq}^{**}} \frac{d\varepsilon_{eq}}{\varepsilon_{eq}^{**}(\eta, \dot{\varepsilon}^{pl})} = 1 \tag{14}$$

where ε_{eq} is the equivalent plastic strain, ε_{eq}^{**} is the equivalent plastic strain at fracture, $\dot{\varepsilon}^{pl}$ is the equivalent plastic strain rate, and η is stress triaxiality that can be calculated by the following equations (Danas and Ponte Castañeda, 2012):

$$\eta = \frac{\sigma_m}{\sigma_{eq}} \tag{15}$$

Here σ_m denotes the hydrostatic stress and σ_{eq} is the Von Mises equivalent stress that can be calculated by the following equations:

$$\sigma_m = \frac{\sigma_{11} + \sigma_{22} + \sigma_{33}}{3} \tag{16}$$

$$\sigma_{eq} = \sqrt{\frac{1}{2}[(\sigma_{11} - \sigma_{22})^2 + (\sigma_{22} - \sigma_{33})^2 + (\sigma_{33} - \sigma_{11})^2 + 6(\sigma_{12}^2 + \sigma_{23}^2 + \sigma_{31}^2)]} \tag{17}$$

As for the Hill's potential function, the stress triaxiality criterion is calculated using the strength values of Table 1.

The damage evolution law describes the rate of degradation of the material stiffness once the corresponding initiation criterion has been reached. For elastoplastic materials, the damage evolution is carried out in two forms: softening of the yield stress and degradation of the elasticity ("Abaqus Analysis User's Manual," 2011). The damage evolution law can be specified either in terms of fracture energy per unit area (G_f) or the equivalent plastic displacement (u^{pl}) which is related to the equivalent plastic strain (ε^{pl}) by the following equation (Venu Gopala Rao et al., 2007):

$$u^{pl} = L_e \varepsilon^{pl} \tag{18}$$

L_e is a characteristic length related to the element. The definition of the characteristic length depends on the element geometry and formulation: it is a typical length of a line across an element for a first-order element, and it is half of the same typical length for a second-order element ("Abaqus Analysis User's Manual," 2011).

The equivalent plastic displacement at failure is computed following the equation (19) where σ_{y0} is the value of the yield strength ("Abaqus Analysis User's Manual," 2011; Venu Gopala Rao et al., 2007).

$$u_f^{pl} = \frac{2\ G_f}{\sigma_{y0}} \tag{19}$$

Table 1: Mechanical properties of elementary flax fibers implemented in the FE model

Property	Direction	Value	Unit	Reference
Stiffness	E_{11} $E_{22} = E_{33}$ $G_{12} = G_{13} = G_{23}$	50 12 3.4	GPa	(Panamoottil et al., 2017)
Poisson ratio	v_{12} $v_{13} = v_{23}$	0.178 0.2	-	
Strength	S_{11} $S_{22} = S_{33}$ $S_{12} = S_{13} = S_{23}$	750 150 20	MPa	

2.3. Finite element modeling of polymer matrix

The two considered matrices (PP and PLA) are modeled in this study with the same elastoplastic behavior and ductile damage criterion as for flax fibers described in Section 2.2. The plastic behavior of the two matrices is also implemented using several points on the yield stress versus plastic strain curve derived from Figure 3. However, the polymer matrices are assumed to have an isotropic behavior and Hill's potential function is not considered for the plastic modeling. It can be noticed that PP and PLA do not generate the same plastic behavior. PP matrix exhibits a high plasticity that reach 40% of strain before failure, while PLA does not exceed 10%. The mechanical parameters considered in model for the two polymer matrices are given in Table 2.

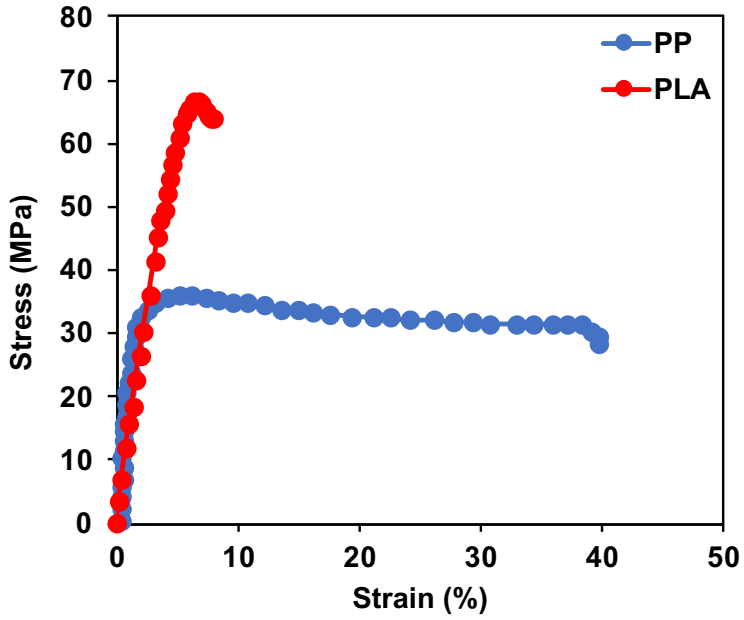

Figure 3: Typical stress/strain curve of PP and PLA (adapted from (Lin et al., 2013) and (Yang et al., 2017))

Table 2: Mechanical properties of polymer matrices implemented in the FE model

Material	Property	Value	Unit	Reference
PP matrix	Stiffness	2.1	GPa	(Lin et al., 2013)
	Poisson ratio	0.4	-	
	Yield stress	35	MPa	
	Strength	30	MPa	
PLA matrix	Stiffness	1.4	GPa	(Yang et al., 2017)
	Poisson ratio	0.35	-	
	Yield stress	50	MPa	
	Strength	64	MPa	

2.4. Finite element modeling of cohesive interfaces

Interfaces are modeled using the cohesive zone model (CZM). The elastic behavior of the CZM is modeled using a linear elastic traction-separation behavior. It assumes initially linear elastic behavior followed by the initiation and evolution of damage. The elastic behavior is

written in terms of an elastic constitutive matrix that relates the nominal stresses to the nominal strains across the interface following the equation ("Abaqus Analysis User's Manual," 2011):

$$\begin{Bmatrix} t_n \\ t_s \\ t_t \end{Bmatrix} = \begin{bmatrix} E_{nn} & E_{ns} & E_{nt} \\ E_{ns} & E_{ss} & E_{st} \\ E_{nt} & E_{st} & E_{tt} \end{bmatrix} \begin{Bmatrix} \varepsilon_n \\ \varepsilon_s \\ \varepsilon_t \end{Bmatrix} \tag{20}$$

Where t_n, t_s and t_t are the nominal stresses in the normal, shear and tangential directions, respectively. E_{ij} are the components of the elasticity matrix. ε_n, ε_s and ε_t are the nominal strains in the normal, shear and tangential directions, respectively. The corresponding separations are denoted by δ_n, δ_s and δ_t and are defined as following, where T_0 is the initial thickness of the cohesive element ("Abaqus Analysis User's Manual," 2011):

$$\varepsilon_n = \frac{\delta_n}{T_0} \tag{21}$$

$$\varepsilon_s = \frac{\delta_s}{T_0} \tag{22}$$

$$\varepsilon_t = \frac{\delta_t}{T_0} \tag{23}$$

In Abaqus software, the penalty stiffness parameter (K_{ij}) is implemented to model the rigidity of the cohesive zone (Camanho et al., 2003; Park et al., 2016) and it is defined by the following equation:

$$\begin{Bmatrix} t_n \\ t_s \\ t_t \end{Bmatrix} = \begin{bmatrix} K_{nn} & K_{ns} & K_{nt} \\ K_{ns} & K_{ss} & K_{st} \\ K_{nt} & K_{st} & K_{tt} \end{bmatrix} \begin{Bmatrix} \delta_n \\ \delta_s \\ \delta_t \end{Bmatrix} \tag{24}$$

Damage of cohesive zones is assumed to initiate when a quadratic interaction function involving the nominal stress ratios reaches a value of one. This criterion can be represented as following ("Abaqus Analysis User's Manual," 2011; Panamoottil et al., 2017):

$$\left(\frac{\langle t_n \rangle}{t_n^0}\right)^2 + \left(\frac{t_s}{t_s^0}\right)^2 + \left(\frac{t_t}{t_t^0}\right)^2 = 1 \tag{25}$$

t_n^0, t_s^0 and t_t^0 are the peak values of the nominal stress components in the normal, shear and tangential directions, respectively. The symbol $\langle\ \rangle$ in the equation (25) represents the Macaulay bracket which is used to signify that a pure compressive deformation or stress state does not initiate damage ("Abaqus Analysis User's Manual," 2011). Table 3 gives the considered mechanical parameters of the cohesive element for both flax/PP and flax/PLA interfaces.

Table 3: Mechanical properties of cohesive interfaces implemented in the FE model

Interface	Property	Direction	Value	Unit	Reference
Flax/PP	Stiffness	$K_{nn} = K_{ss} = K_{tt}$ $K_{ns} = K_{nt} = K_{st}$	27.96 0	GPa/mm	(Panamoottil et al., 2017)
	Strength	$t_n^0 = t_s^0 = t_t^0$	28.5	MPa	
	Fracture energy	G^C	4	J/m^2	
Flax/PLA	Stiffness	$K_{nn} = K_{ss} = K_{tt}$ $K_{ns} = K_{nt} = K_{st}$	38 0	GPa/mm	Calculated from data of (Le Duigou et al., 2014)
	Strength	$t_n^0 = t_s^0 = t_t^0$	18	MPa	(Le Duigou et al., 2014, 2010)
	Fracture energy	G^C	28	J/m^2	

3. Experimental validation

The experimental validation of the FE model has been performed using orthogonal cutting process on both flax/PP and flax/PLA composites. The two NFC samples are manufactured by thermocompression of unidirectional flax fabrics and polymer matrix. Flax fabrics are based on technical fibers that are a bundle of about 3 to 6 elementary fibers.

Orthogonal cutting tests are performed on a shaper machine (GSP – EL 136) with a carbide cutting insert (Sandvik – TCGX 16 T3 04 – AL H10) as shown in Figure 4. The machining forces are acquired using a piezoelectric dynamometer (Kistler – 9255B). The machined surfaces are then observed at microscale using the scanning electron microscope (SEM) at

low vacuum mode (JEOL – 5510LV). To ensure the repeatability of the experimental outputs, each cutting configuration is tested three times. Thus, the final outputs from the orthogonal cutting experiments are presented as the mean value of these three repeated tests. Measurement errors are considered as the average of the absolute deviations of data repeatability tests from their mean.

The cutting experiments on flax/PP samples have been devoted to investigating the effect of cutting speed (V_c). Therefore, the cutting speed has been varied from 12 m/min to 80 m/min. On the other side, the cutting experiments on flax/PLA samples concerned the study of the fiber orientation effect (θ). To this aim, the orientation of flax fibers, with respect to the cutting direction, has been varied from 0° to 90°. Table 4 summarizes the experimental cutting conditions related to the tool geometry, tool kinematic, and the process parameters. The FE model was performed with the same cutting conditions.

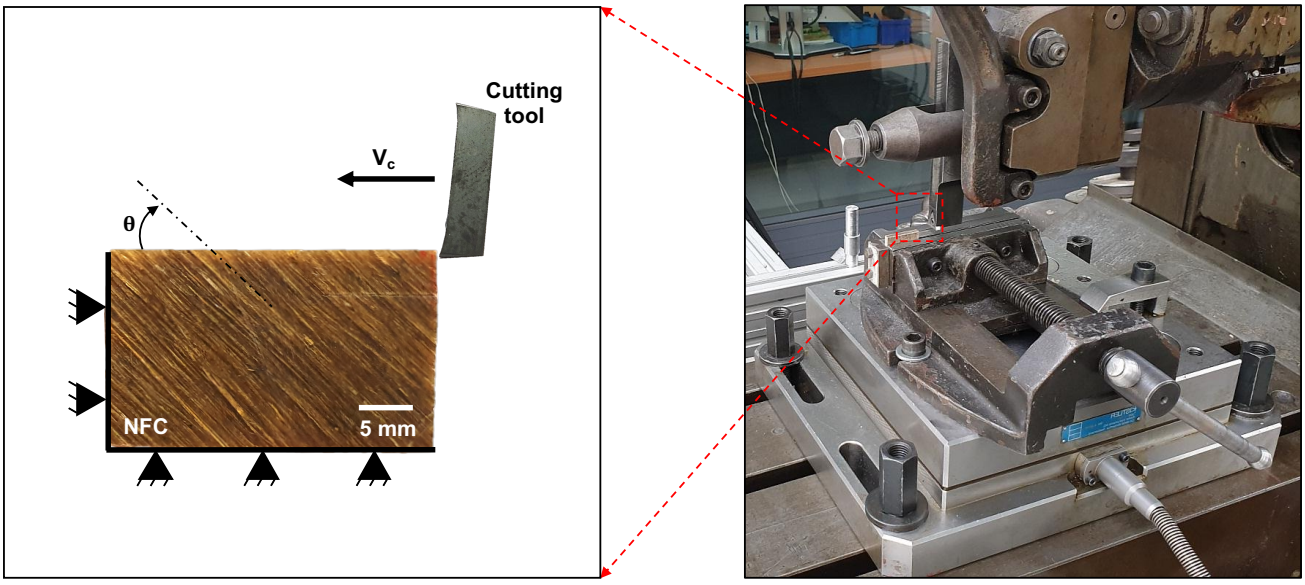

Figure 4: Photographic image of the experimental setup with a zoom on the active zone of tool/material interaction

Table 4: Experimental cutting condition for orthogonal cutting tests

		Parameter	Value	Unit
Tool geometry		Rake angle (γ) Clearance angle (α) Edge radius (r_ε)	20 7 12	Degree (°) Degree (°) µm
Cutting parameters	**Flax/PP cutting**	Depth of cut (a_p) Fiber orientation Cutting speed (V_c)	100 90 12 / 20 / 32 / 50 / 80	µm ° m/min
	Flax/PLA cutting	Depth of cut (a_p) Fiber orientation Cutting speed (V_c)	100 0 / 25 / 45 / 65 / 90 50	µm ° m/min

4. Numerical effect of cutting speed

The numerical investigation of the effect of cutting speed has been performed on flax/PP composites with a fiber orientation of 90º from the cutting direction (Chegdani et al., 2019b). Figure 5 presents the comparison between the numerical and the experimental machining results of flax/PP at low cutting speed (12 m/min) and high cutting speed (80 m/min). It can be noticed a significant impact of the cutting speed on the cutting behavior of flax fibers inside the composite. Cutting with low cutting speed induced high transverse plastic deformation of flax fibers toward the cutting direction. Flax fibers are then torn off rather than sheared as shown in Figure 5(a,c). Consequently, high decohesion zones are produced because of interfaces damage. When increasing the cutting speed to high values, flax fibers are sheared efficiently thanks to the increase of the contact stiffness. Flax fibers are then less deformed and the decohesion zones are strongly reduced as shown in Figure 5(b,d). All these cutting phenomena related the cutting speed effect are reproduced by the FE model that shows also a less induced subsurface damage when cutting with high cutting speed.

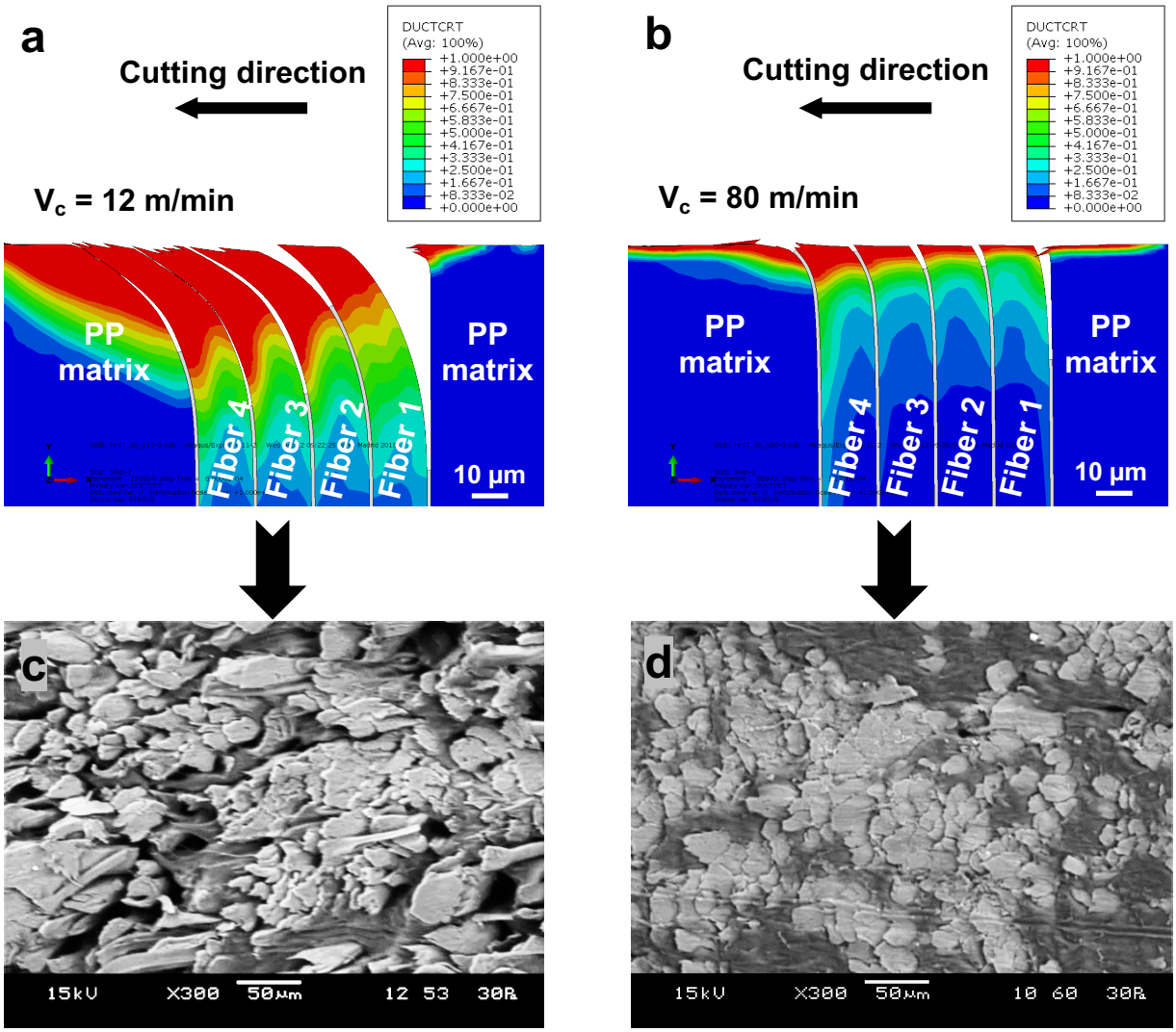

Figure 5: Numerical and experimental cutting behavior of flax fibers within the flax/PP composite at low and high cutting speed.

Figure 6 presents a comparison between the experimental and the numerical machining forces obtained for the orthogonal cutting of flax/PP composites. The numerical cutting forces correspond to the experimental ones in terms of trend and magnitude where the cutting forces increase by increasing the cutting speed (Figure 6(a)). For the thrust forces, the numerical outputs correspond to the experimental ones in terms of trend. However, there is a factor of 3 between the experimental and the numerical values as clearly shown in Figure 6(b). This correlation issue is well known also in FE machining models of synthetic fiber composites (Arola and Ramulu, 1997; Lasri et al., 2009) and it can be due to the fibers spring-back as reported in (Lasri et al., 2009). The magnitude factor between simulation and experimental

thrust forces in around 8.5 in (Arola and Ramulu, 1997) and around 9.33 in (Lasri et al., 2009) for the same considered fiber orientation (90°). The magnitude factor of 3 found in the current model for machining NFC is less than those of the synthetic fiber composite model because natural fibers have less spring-back intensity due to their high transverse elasticity (Chegdani et al., 2019b). Therefore, next section will address this correlation issue through a tribological approach based on the friction properties of the tool/NFC cutting contact.

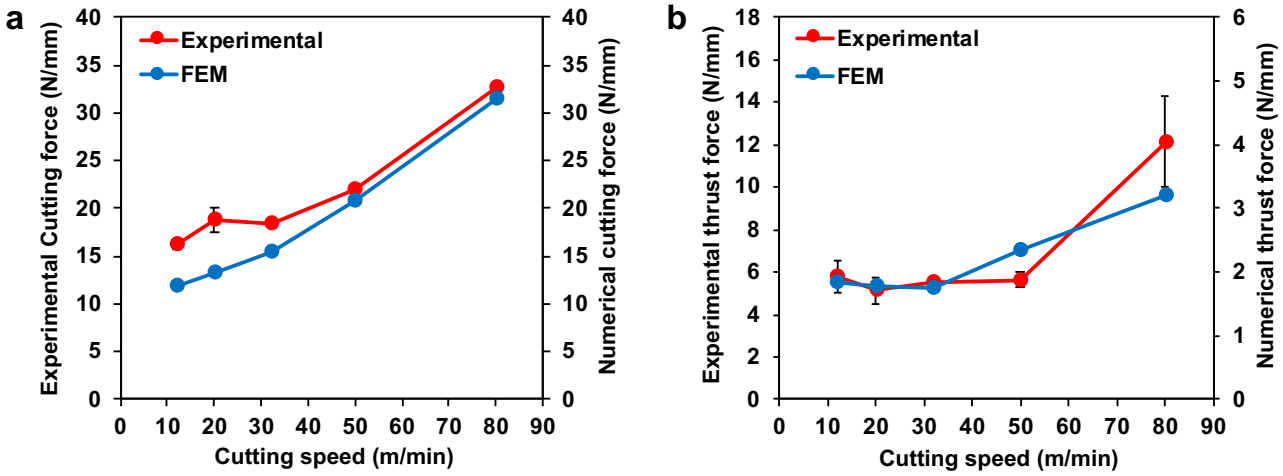

Figure 6: Comparison between numerical and experimental machining forces for flax/PP composites. (a) cutting forces, (b) thrust forces

5. Numerical effect of the local cutting friction

In section 4, the FE model shows correlation issues of the thrust forces that can be due to the spring-back phenomenon of fibers during the cutting operation. However, no theoretical or experimental evidence can confirm this hypothesis. For this reason, a different approach is investigated in this section to address the issue of the thrust force correlation in the FE modeling of NFRP machining. This approach is based on the machining tribology, especially the micro-friction between the composite and the cutting tool. The micro-friction means the local friction between the cutting tool and each composite phase component at microscale (elementary natural fibers and polymer matrix). The considered investigation is motivated by previous works on the local micro-friction on NFC composites by scratch-test experiments

(Chegdani et al., 2019a, 2018b). Indeed, the first scratch-test experiments were done with a diamond Berkovich tip indenter and the friction coefficient has been found around 0.4 for polypropylene (PP) matrix and around 0.5 for flax fibers (Chegdani et al., 2018b). These values were used in the previous FE model of machining (Chegdani et al., 2019b). However, the following scratch-test experiments were done with a Sapphire Berkovich tip indenter and the friction coefficient has been found around 0.2 for both PP matrix and flax fibers at the same scratching conditions as the experiments with the diamond indenter (Chegdani et al., 2019a). This indicates that the tool material causes a significant modification of the frictional properties in the case of NFRP composites. Therefore, the values of the micro-friction used in the previous FE machining model may be not appropriate because the experimental machining tests were performed by a carbide cutting insert. This could be the origin of the magnitude difference in the thrust forces of the FE machining model.

To this aim, the FE micromechanical model is used in this section for flax/PLA composites to investigate the effect of the local micro-friction on the cutting behavior for different fiber orientation values.

To simulate the orthogonal cutting friction with ABAQUS/CAE software in the micromechanical FE model, a penalty contact method is considered to define each contact interaction ("Abaqus Analysis User's Manual," 2011). This method is based on Coulomb friction law to control the frictional contacts between the cutting tool and the composite. Coulomb friction law assumes that relative motion between the tool and the composite occurs at the contact point when the equivalent shear stress along the tool-material interface (τ_f) is more than or equal to the critical friction stress as follows:

$$\tau_f \geq \tau_{crit} = \mu\, n_p \tag{26}$$

Where μ is the friction coefficient and n_p is the normal pressure at the same point.

The notion of friction in the FE model is based on the interaction between the nodes of the too surfaces in contact. Since the developed model is performed at microscale, the friction coefficient needed for the micromechanical model should be the local micro-friction coefficient at each point of the cutting contact. Thus, the micromechanical model will differentiate two contact pairs with the cutting tool because elementary flax fibers and PLA matrix are modeled separately. Consequently, two micro-friction parameters will be considered in this study:

- The micro-friction coefficient of the contact between the cutting tool and flax fibers (μ_f)
- The micro-friction coefficient of the contact between the cutting tool and PLA matrix (μ_m)

The tested values of micro-friction coefficients has been chosen ta vary from 0.1 to 0.5 based on the results of the scratch-test experiments (Chegdani et al., 2019a, 2017).

Figure 7 shows the comparison between numerical and experimental machining forces with different valuers of micro-friction coefficients. In each graph of Figure 7, the micro-friction coefficient of the PLA matrix (μ_m) is kept constant, and the micro-friction coefficient of flax fibers (μ_f) is variated from 0.1 to 0.5 in order to evaluate its effect on the numerical machining forces.

Generally, the cutting forces are not significantly affected by the variation of the numerical micro-friction coefficients. As for the numerical results of Figure 6, the numerical cutting forces correspond to the experimental outputs in terms of trend and magnitude as shown in Figure 7(a,c,e).

On the other side, the numerical thrust force outputs are highly dependent on the variation of the micro-friction coefficients in the FE model. Indeed, when performing the FE simulations with μ_m = 0.1, it can be seen in Figure 7(b) that numerical thrust forces are closer to the experimental ones at the lowest value of micro-friction coefficient of flax fibers with the cutting

tool (μ_f = 0.1). Increasing μ_f provokes o deviation of the numerical thrust forces from the experimental outputs.

Furthermore, Increasing the value of μ_m leads to rise the divergence between the numerical and the experimental values of thrust forces (Figure 7(b→d→f)). Therefore, Figure 7 indicates that the FE model can reproduce the experimental outputs with good accuracy for an isotropic micro-friction where $\mu_f = \mu_m = 0.1$.

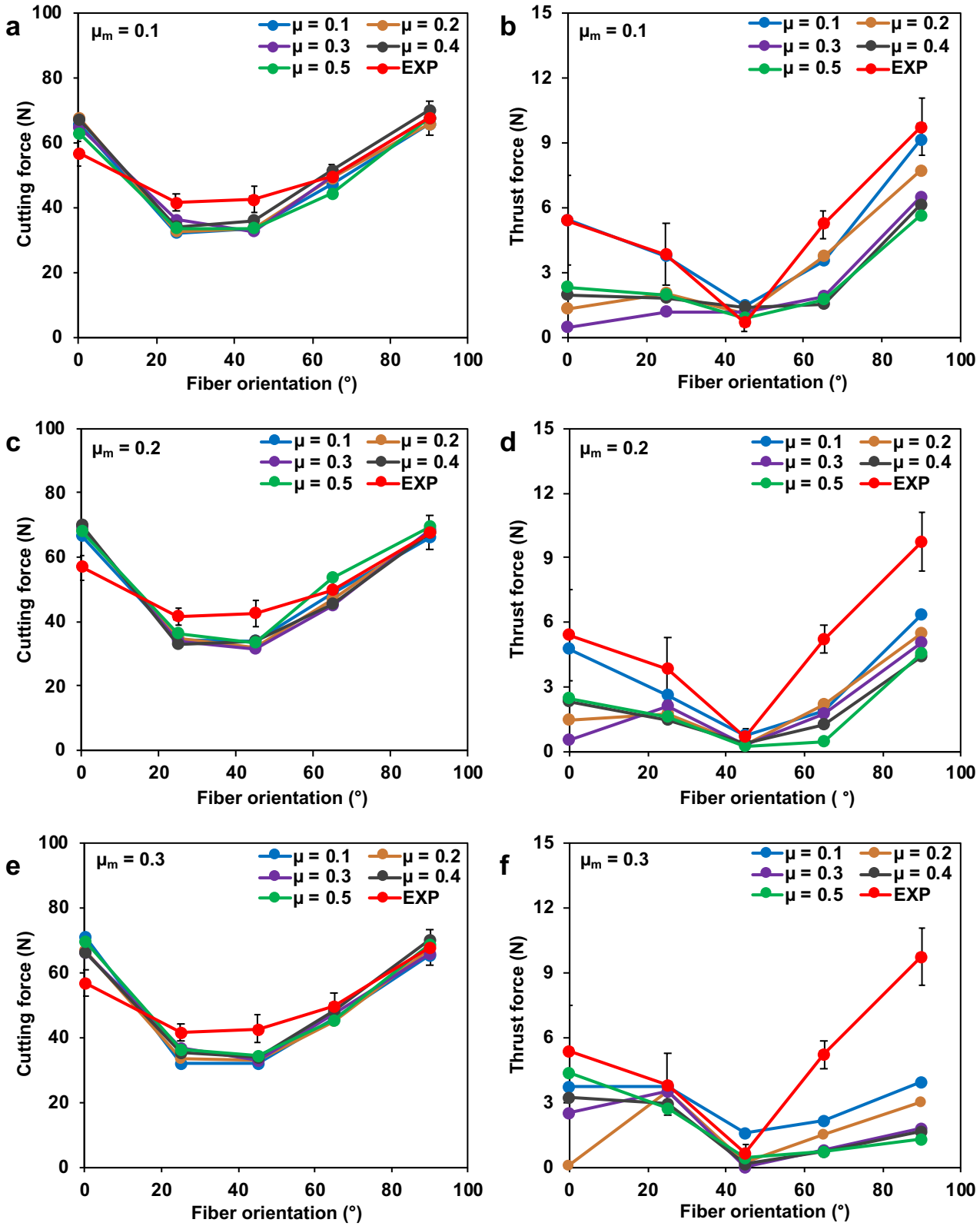

Figure 7: Comparison between experimental and numerical machining forces at different values of micro-friction. (a,c,e) cutting forces and (b,d,f) thrust forces. μ in the graphs corresponds to μ_f

6. Numerical effect of fiber orientation

In this section, the numerical simulations are performed with an isotropic micro-friction coefficient of 0.1 as suggested by the tribological investigation of Section 5. Figure 8 presents a comparison between the numerical and the experimental cutting behavior of flax fibers inside the PLA matrix at different values of fiber orientation. Cutting with θ = 25º induces the highest ductile damages caused by plastic deformation as shown in Figure 8(a). These damages weaken the fiber shearing which is clearly obvious in SEM image of Figure 8(b) where flax fibers are so deformed that it is not possible to distinguish the elementary fibers in each fibers bundle.

When changing the fiber orientation from 25º to 45º, ductile damages are reduced which enhance the shearing of flax fibers as shown in Figure 8(c). The same finding is noticed in the corresponding SEM image of Figure 8(d) when elementary flax fibers becomes slightly visible due to the decrease of plastic deformation when cutting.

At θ = 65º, Figure 8(e) the ductile damages are significantly reduced and the fiber shearing are strengthened which corresponds to the experimental observation of Figure 8(f) where no significant plastic deformation of flax fibers is noticed and the cross-sections of elementary fibers are clearly visible.

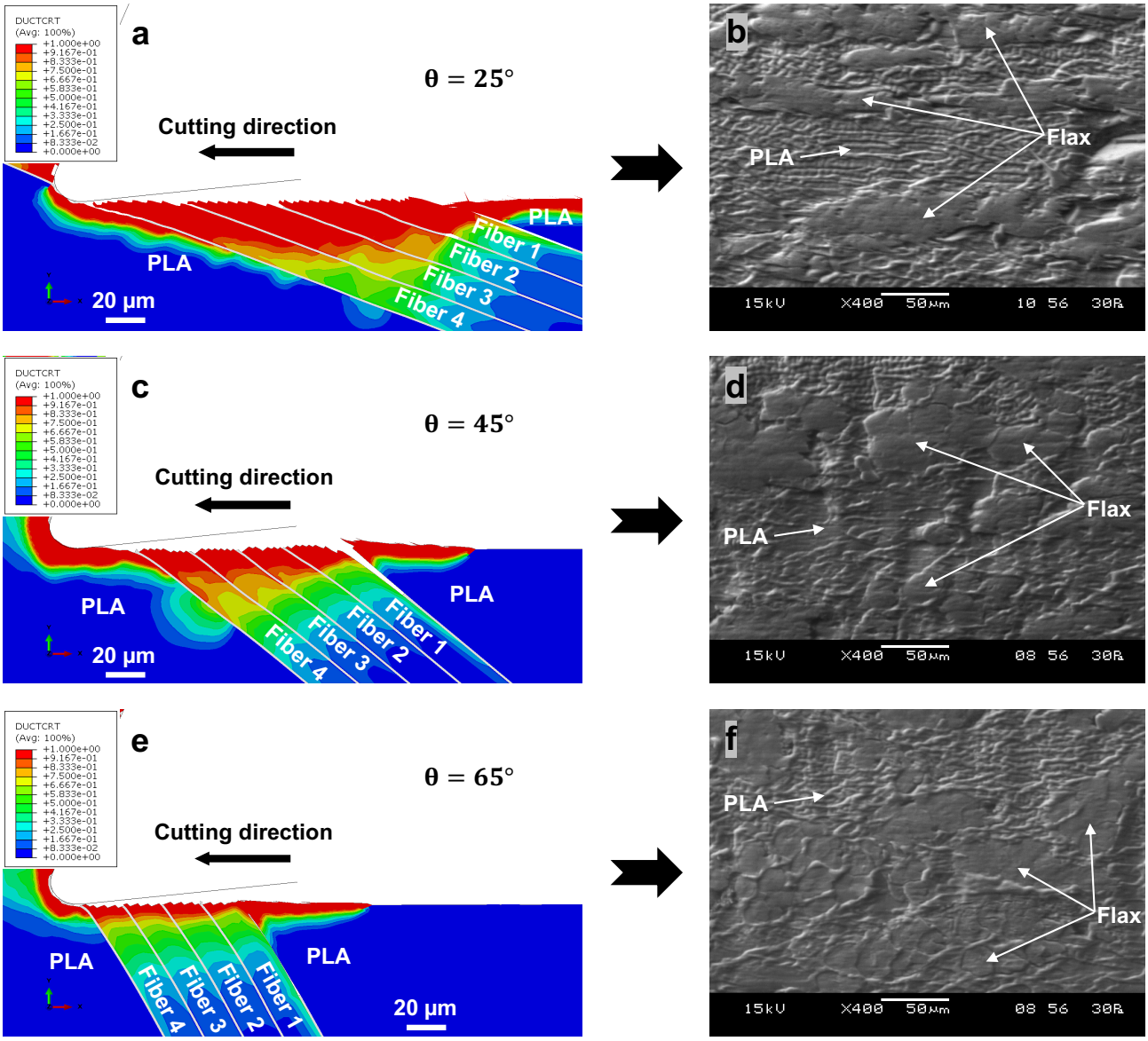

Figure 8: Numerical and experimental cutting behavior of flax fibers within the flax/PLA composite at different values of fiber orientation

7. Conclusions

In this chapter, a 2D finite element model is developed to simulate the machining behavior of natural fiber composites at the microscopic scale of natural fibers. Flax fiber reinforced polypropylene and flax fiber reinforced polylactic-acid are considered to perform the experimental validation using the fundamental process of orthogonal cutting. Cutting speed and fiber orientation parameters are used to investigate the predictiveness accuracy of the FE model. The following conclusions can be drawn:

- Unlike synthetic fibers such as glass and carbon, natural fibers should be modeled with an elasto-plastic behavior and a ductile criterion for failure.
- The FE model is able to predict with good accuracy the qualitative cutting behavior of flax fibers inside the polymer matrix.
- The FE model can predict with good accuracy the cutting forces. However, the thrust forces are predicted with a deviation in the magnitude.
- The magnitude predictiveness issue of thrust forces is optimized by investigations the local micro-friction between the cutting tool on each composite component at microscale. It has been found that an isotropic micro-friction coefficient of 0.1 provides a good predictiveness of the thrust forces.

8. References

Abaqus Analysis User's Manual, 2011. , in: Abaqus 6.11 Documentation. Dassault Systèmes Simulia Corp., Providence, RI, USA.

Arola, D., Ramulu, M., 1997. Orthogonal cutting of fiber-reinforced composites: A finite element analysis. Int. J. Mech. Sci. 39, 597–613. https://doi.org/10.1016/S0020-7403(96)00061-6

Baley, C., 2002. Analysis of the flax fibres tensile behaviour and analysis of the tensile stiffness increase. Compos. - Part A Appl. Sci. Manuf. 33, 939–948. https://doi.org/10.1016/S1359-835X(02)00040-4

Camanho, P.P., Davila, C.G., de Moura, M.F., 2003. Numerical Simulation of Mixed-Mode Progressive Delamination in Composite Materials. J. Compos. Mater. 37, 1415–1438. https://doi.org/10.1177/0021998303034505

Cardoso, R.P.R., Adetoro, O.B., 2017. A generalisation of the Hill's quadratic yield function for planar plastic anisotropy to consider loading direction. Int. J. Mech. Sci. 128–129, 253–268. https://doi.org/10.1016/j.ijmecsci.2017.04.024

Charlet, K., Baley, C., Morvan, C., Jernot, J.P., Gomina, M., Bréard, J., 2007. Characteristics of Hermès flax fibres as a function of their location in the stem and properties of the derived unidirectional composites. Compos. Part A Appl. Sci. Manuf. 38, 1912–1921. https://doi.org/10.1016/j.compositesa.2007.03.006

Chegdani, F., El Mansori, M., 2019. New Multiscale Approach for Machining Analysis of Natural Fiber Reinforced Bio-Composites. J. Manuf. Sci. Eng. Trans. ASME 141, 11004. https://doi.org/10.1115/1.4041326

Chegdani, F., El Mansori, M., 2018. Friction scale effect in drilling natural fiber composites. Tribol. Int. 119, 622–630. https://doi.org/10.1016/j.triboint.2017.12.006

Chegdani, F., El Mansori, M., Bukkapatnam, S.T.S., El Amri, I., 2019a. Thermal effect on

the tribo-mechanical behavior of natural fiber composites at micro-scale. Tribol. Int. https://doi.org/10.1016/j.triboint.2019.06.024

Chegdani, F., El Mansori, M., Mezghani, S., Montagne, A., 2017. Scale effect on tribo-mechanical behavior of vegetal fibers in reinforced bio-composite materials. Compos. Sci. Technol. 150, 87–94. https://doi.org/10.1016/j.compscitech.2017.07.012

Chegdani, F., El Mansori, M., T. S. Bukkapatnam, S., Reddy, J.N., 2019b. Micromechanical modeling of the machining behavior of natural fiber-reinforced polymer composites. Int. J. Adv. Manuf. Technol. 105, 1549–1561. https://doi.org/10.1007/s00170-019-04271-3

Chegdani, F., Mansori, M. El, 2018. Mechanics of material removal when cutting natural fiber reinforced thermoplastic composites. Polym. Test. 67, 275–283. https://doi.org/10.1016/j.polymertesting.2018.03.016

Chegdani, F., Mezghani, S., El Mansori, M., 2016. On the multiscale tribological signatures of the tool helix angle in profile milling of woven flax fiber composites. Tribol. Int. 100, 132–140. https://doi.org/10.1016/j.triboint.2015.12.014

Chegdani, Faissal, Mezghani, S., El Mansori, M., 2015. Experimental study of coated tools effects in dry cutting of natural fiber reinforced plastics. Surf. Coatings Technol. 284, 264–272. https://doi.org/10.1016/j.surfcoat.2015.06.083

Chegdani, F., Mezghani, S., El Mansori, M., Mkaddem, A., 2015. Fiber type effect on tribological behavior when cutting natural fiber reinforced plastics. Wear 332–333, 772–779. https://doi.org/10.1016/j.wear.2014.12.039

Chegdani, F., Takabi, B., Tai, B.L., Mansori, M. El, Bukkapatnam, S.T.S., 2018a. Thermal Effects on Tribological Behavior in Machining Natural Fiber Composites. Procedia Manuf. 26, 305–316. https://doi.org/10.1016/j.promfg.2018.07.039

Chegdani, F., Wang, Z., El Mansori, M., Bukkapatnam, S.T.S., 2018b. Multiscale tribo-mechanical analysis of natural fiber composites for manufacturing applications. Tribol.

Int. 122, 143–150. https://doi.org/10.1016/j.triboint.2018.02.030

Danas, K., Ponte Castañeda, P., 2012. Influence of the Lode parameter and the stress triaxiality on the failure of elasto-plastic porous materials. Int. J. Solids Struct. 49, 1325–1342. https://doi.org/10.1016/J.IJSOLSTR.2012.02.006

Dandekar, C.R., Shin, Y.C., 2012. Modeling of machining of composite materials: A review. Int. J. Mach. Tools Manuf. 57, 102–121. https://doi.org/10.1016/j.ijmachtools.2012.01.006

Dandekar, C.R., Shin, Y.C., 2008. Multiphase Finite Element Modeling of Machining Unidirectional Composites: Prediction of Debonding and Fiber Damage. J. Manuf. Sci. Eng. 130, 51016. https://doi.org/10.1115/1.2976146

Dittenber, D.B., GangaRao, H.V.S., 2012. Critical review of recent publications on use of natural composites in infrastructure. Compos. Part A Appl. Sci. Manuf. https://doi.org/10.1016/j.compositesa.2011.11.019

Gao, C., Xiao, J., Xu, J., Ke, Y., 2016. Factor analysis of machining parameters of fiber-reinforced polymer composites based on finite element simulation with experimental investigation. Int. J. Adv. Manuf. Technol. 83, 1113–1125. https://doi.org/10.1007/s00170-015-7592-2

Hooputra, H., Gese, H., Dell, H., Werner, H., 2004. A comprehensive failure model for crashworthiness simulation of aluminium extrusions. Int. J. Crashworthiness 9, 449–464. https://doi.org/10.1533/ijcr.2004.0289

Hossain, R., Islam, A., Vuure, A. Van, Verpoest, I., 2013. Processing dependent flexural strength variation of jute fiber reinforced epoxy composites. J. Eng. Appl. Sci. 8, 513–518.

Johnson, G.R., Cook, W.H., 1985. Fracture characteristics of three metals subjected to various strains, strain rates, temperatures and pressures. Eng. Fract. Mech. 21, 31–48.

https://doi.org/10.1016/0013-7944(85)90052-9

Keryvin, V., Lan, M., Bourmaud, A., Parenteau, T., Charleux, L., Baley, C., 2015. Analysis of flax fibres viscoelastic behaviour at micro and nano scales. Compos. Part A Appl. Sci. Manuf. 68, 219–225. https://doi.org/10.1016/j.compositesa.2014.10.006

Lasri, L., Nouari, M., El Mansori, M., 2009. Modelling of chip separation in machining unidirectional FRP composites by stiffness degradation concept. Compos. Sci. Technol. 69, 684–692. https://doi.org/10.1016/J.COMPSCITECH.2009.01.004

Le Duigou, A., Baley, C., Grohens, Y., Davies, P., Cognard, J.-Y., Créach'cadec, R., Sohier, L., 2014. A multi-scale study of the interface between natural fibres and a biopolymer. Compos. Part A Appl. Sci. Manuf. 65, 161–168. https://doi.org/10.1016/J.COMPOSITESA.2014.06.010

Le Duigou, A., Davies, P., Baley, C., 2010. Interfacial bonding of Flax fibre/Poly(l-lactide) bio-composites. Compos. Sci. Technol. 70, 231–239. https://doi.org/10.1016/J.COMPSCITECH.2009.10.009

Lin, S., Xia, Y., Lin, C., Wang, J., Gu, G., 2013. Stress State Dependent Failure Loci of a Talc-filled Polypropylene Material under Static Loading and Dynamic Loading, in: 13th International Conference on Fracture. Beijing, pp. 1–16.

Lotfi, A., Li, H., Dao, D.V., Prusty, G., 2019. Natural fiber–reinforced composites: A review on material, manufacturing, and machinability. J. Thermoplast. Compos. Mater. 089270571984454. https://doi.org/10.1177/0892705719844546

Nassar, M.M.A., Arunachalam, R., Alzebdeh, K.I., 2017. Machinability of natural fiber reinforced composites: a review. Int. J. Adv. Manuf. Technol. 88, 2985–3004. https://doi.org/10.1007/s00170-016-9010-9

Nayak, D., Singh, I., Bhatnagar, N., Mahajan, P., 2004. An Analysis of Machining Induced Damages in FRP Composites — A Micromechanics Finite Element Approach, in: AIP

Conference Proceedings. AIP, pp. 327–331. https://doi.org/10.1063/1.1766545

Panamoottil, S.M., Das, R., Jayaraman, K., 2017. Towards a multiscale model for flax composites from behaviour of fibre and fibre/polymer interface. J. Compos. Mater. 51, 859–873. https://doi.org/10.1177/0021998316654303

Park, K., Choi, H., Paulino, G.H., 2016. Assessment of cohesive traction-separation relationships in ABAQUS: A comparative study. Mech. Res. Commun. 78, 71–78. https://doi.org/10.1016/J.MECHRESCOM.2016.09.004

Placet, V., Cissé, O., Lamine Boubakar, M., 2014. Nonlinear tensile behaviour of elementary hemp fibres. Part I: Investigation of the possible origins using repeated progressive loading with in situ microscopic observations. Compos. Part A Appl. Sci. Manuf. 56, 319–327. https://doi.org/10.1016/J.COMPOSITESA.2012.11.019

Rajmohan, T., Vinayagamoorthy, R., Mohan, K., 2019. Review on effect machining parameters on performance of natural fibre–reinforced composites (NFRCs). J. Thermoplast. Compos. Mater. 32, 1282–1302. https://doi.org/10.1177/0892705718796541

Rao, G.V.G., Mahajan, P., Bhatnagar, N., 2007. Micro-mechanical modeling of machining of FRP composites – Cutting force analysis. Compos. Sci. Technol. 67, 579–593. https://doi.org/10.1016/j.compscitech.2006.08.010

Roy Choudhury, M., Srinivas, M.S., Debnath, K., 2018. Experimental investigations on drilling of lignocellulosic fiber reinforced composite laminates. J. Manuf. Process. 34, 51–61. https://doi.org/10.1016/J.JMAPRO.2018.05.032

Santiuste, C., Soldani, X., Miguélez, M.H., 2010. Machining FEM model of long fiber composites for aeronautical components. Compos. Struct. 92, 691–698. https://doi.org/10.1016/J.COMPSTRUCT.2009.09.021

Shah, D.U., Schubel, P.J., Licence, P., Clifford, M.J., 2012. Determining the minimum,

critical and maximum fibre content for twisted yarn reinforced plant fibre composites. Compos. Sci. Technol. 72, 1909–1917. https://doi.org/10.1016/J.COMPSCITECH.2012.08.005

Venu Gopala Rao, G., Mahajan, P., Bhatnagar, N., 2007. Machining of UD-GFRP composites chip formation mechanism. Compos. Sci. Technol. 67, 2271–2281. https://doi.org/10.1016/J.COMPSCITECH.2007.01.025

Vinayagamoorthy, R., Rajmohan, T., 2018. Machining and its challenges on bio-fibre reinforced plastics: A critical review. J. Reinf. Plast. Compos. 37, 1037–1050. https://doi.org/10.1177/0731684418778356

Yang, J., Pan, H., Li, X., Sun, S., Zhang, H., Dong, L., 2017. A study on the mechanical, thermal properties and crystallization behavior of poly(lactic acid)/thermoplastic poly(propylene carbonate) polyurethane blends. RSC Adv. 7, 46183–46194. https://doi.org/10.1039/C7RA07424G